J. Sens. Sens. Syst., 7, 101–111, 2018
https://doi.org/10.5194/jsss-7-101-2018

JSSS Journal of Sensors and Sensor Systems Open Access

Design and evaluation of split-ring resonators for aptamer-based biosensors

Tobias Reinecke[1], Johanna-Gabriela Walter[2], Tim Kobelt[1], André Ahrens[1], Thomas Scheper[2], and Stefan Zimmermann[1]

[1]Leibniz Universität Hannover, Institute of Electrical Engineering and Measurement Technology, Department of Sensors and Measurement Technology, Appelstr. 9A, 30167 Hanover, Germany
[2]Institute of Technical Chemistry, Leibniz Universität Hannover, Callinstr. 5, 30167 Hanover, Germany

Correspondence: Tobias Reinecke (reinecke@geml.uni-hannover.de)

Received: 29 September 2017 – Revised: 6 January 2018 – Accepted: 9 January 2018 – Published: 23 February 2018

Abstract. Split-ring resonators are electrical circuits, which enable highly sensitive readout of split capacity changes via a measurement of the shift in the resonance frequency. Thus, functionalization of the split allows the development of biosensors, where selective molecular binding causes a change in permittivity and therefore a change in split capacity. In this work, we present a novel approach using transmission line theory to describe the dependency between permittivity of the sample and resonance frequency. This theory allows the identification of all relevant parameters of a split-ring resonator and thus a target-oriented optimization process. Hereby all setup optimizations are verified with measurements. Subsequently, the split of a resonator is functionalized with aptamers and the sensor response is investigated. This preliminary experiment shows that introducing the target protein results in a shift in the resonance frequency caused by a permittivity change due to aptamer-mediated protein binding, which allows selective detection of the target protein.

1 Introduction

Split-ring resonators originate from the field of metamaterials, as they can exhibit effects like negative permittivity and permeability (Smith et al., 2000). However, in recent years, there is an increasing use of split-ring resonators in sensor and measuring technology, as they allow highly sensitive detection of changes in the polarizability (permittivity) of a material via the detection of a shift in the resonance frequency. Split-ring resonators are employed in a broad field of applications (Schueler et al., 2012). There are systems described in literature, e.g., for dielectric characterization of liquids (Ebrahimi et al., 2014) or analysis of organic tissues (Puentes et al., 2011). Furthermore, they are found useful for measuring physical values like distance and rotation (Naqui et al., 2011). Another field of application is material testing for the detection of cracks in metal (Albishi and Ramahi, 2014).

Additionally, there are already some biosensors based on split-ring resonators described in literature. In Lee and Yook (2008) they are used for the detection of biotin and streptavidin binding, in Lee et al. (2012) for the detection of prostate-specific antigen and in Jaruwongrungsee et al. (2015) for the detection of immunoglobulin. Furthermore, observation of DNA hybridization is reported in Lee et al. (2010).

However, all described resonator structures differ significantly, e.g., in size, shape and used materials, complicating the comparison of sensor performance. Based on our initial paper (Reinecke et al., 2017), the aim of this work is to present a new theory for the dependency of resonance frequency and sample permittivity. Subsequently, this theory is used to perform target-oriented parametric studies to realize a split-ring resonator exhibiting maximum sensitivity. Preliminary results of a first aptamer-functionalized split-ring resonator for the label-free detection of C-reactive protein (CRP) are presented.

2 Fundamentals

Figure 1 shows the basic structure of a split-ring resonator. The used printed circuit board (PCB) is a 3 mm thick FR4

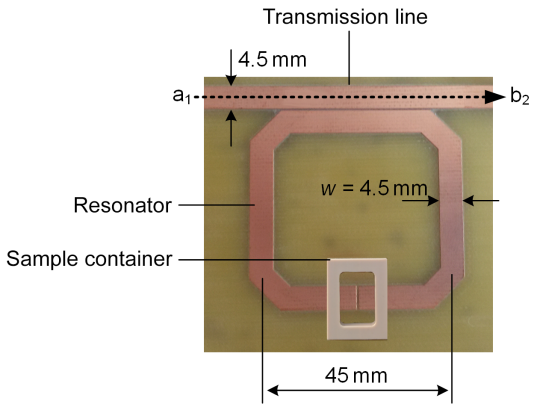

Figure 1. PCB with split-ring resonator.

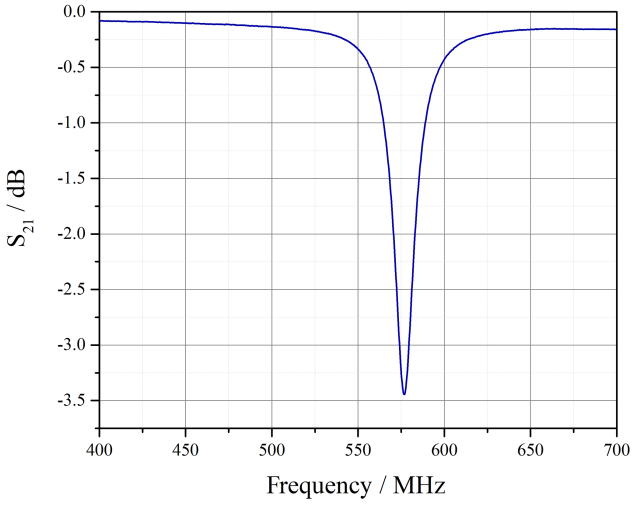

Figure 2. Transmission measurement of the unloaded split-ring resonator.

substrate with a ground plane on the backside. The structure on the top layer consists of a transmission line with a width of 4.5 mm resulting in a wave impedance of 50 Ω. Furthermore, a square resonator structure with a mean edge length of 45 mm is located in a small distance of 300 µm. The edges of the resonator structure are cut off to reduce fringe effects. In a previous work, the square structure was found to be superior to a round structure, as it leads to a better coupling between resonator and transmission line, combined with a high Q factor (Reinecke et al., 2016). Opposite to the transmission line, there is a split in the resonator structure with a sample container placed on top of it.

The split-ring resonator is characterized via a transmission measurement ($S_{21} = b_2/a_1$), i.e., the amplitude ratio of the received wave b_2 and the transmitted wave a_1. The S_{21} dependent on the frequency for the depicted unloaded resonator (loaded with air respectively) is shown in Fig. 2. Hereby, the resonance frequency is found at the lowest S_{21} value.

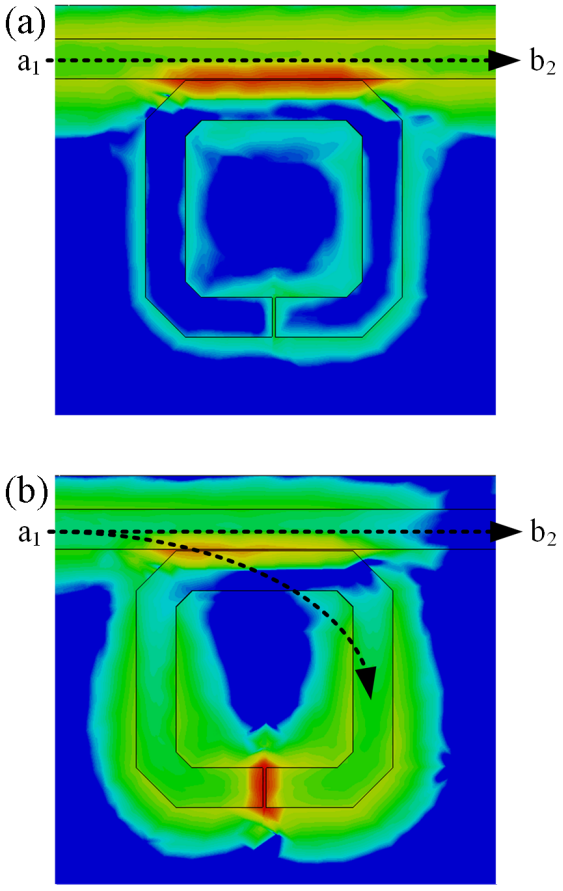

Figure 3. CST Microwave Studio simulation of the split-ring resonator outside resonance **(a)** and in resonance **(b)**.

The electromagnetic behavior of the resonator can be visualized via FEM (finite element method) simulations as depicted in Fig. 3. Outside of resonance, the resonator structure is virtually field-free and thus all power is transmitted from transmitter to receiver ($a_1 = b_2$). However, in resonance, the wave couples into the resonator structure, where a standing wave is formed. Therefore, there is a high field strength in the ring, especially in the split (see Fig. 3b), and thus power transmission from transmitter to receiver is drastically diminished ($a_1 > b_2$).The resonance frequency partly depends on the circumference of the resonator, while a bigger circumference leads to a lower resonance frequency and, furthermore, the resonance frequency is determined by the capacity of the split.

3 New theory for the relation between relative sample permittivity and resonance frequency

The influence of the capacity on the resonance frequency can be qualitatively explained with the same mechanisms leading to an extension of the electrical length of half-wave dipoles due to hat capacitances (top hats) in antenna tech-

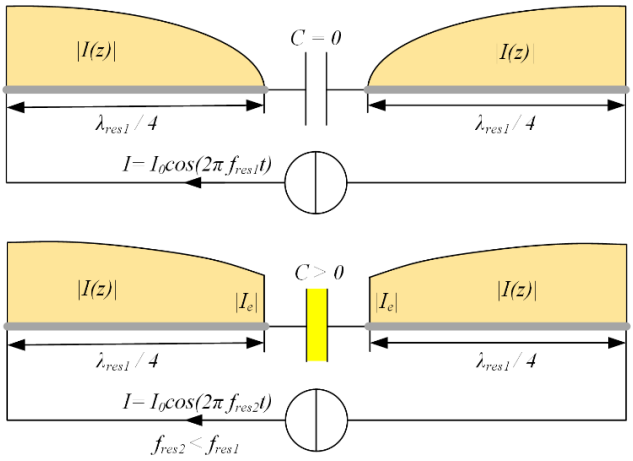

Figure 4. Current distribution in the resonator structure in resonance for a hypothetical split capacity $C = 0$ (top) and $C > 0$ (bottom).

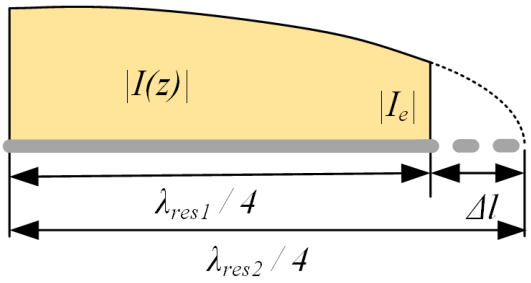

Figure 5. A capacitive load leads to an extension of the electrical length of the resonator.

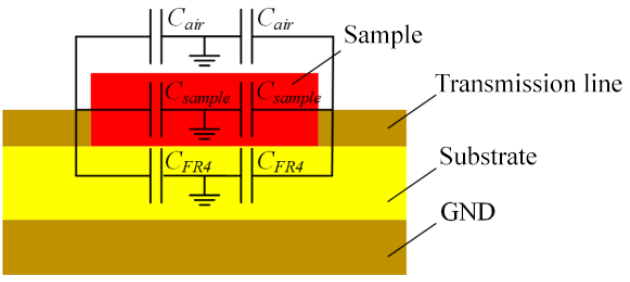

Figure 6. Cross section of the split capacity.

nology (Rudge et al., 1983; Huang and Boyle, 2008). However, the commonly used assumptions for describing this phenomenon are only valid for very small extensions of the electrical length and thus cannot be applied for the description of a split-ring resonator. Therefore, a new theory based on transmission line theory to describe the relation between relative sample permittivity and resonance frequency is presented in the following.

The relative permittivity is generally a complex value $\varepsilon_\mathrm{r} = \varepsilon_\mathrm{r}' - j\varepsilon_\mathrm{r}''$. The real part of the relative permittivity ε_r' is a measure for the polarizability of a material and the imaginary part ε_r'' a measure for dielectric or conductive losses. The following theory only considers the frequency shift due to a change in the polarizability of the material (ε_r'). However, the influence of dielectric losses is accounted for by using the natural frequency (undamped resonator) instead of the measured resonance frequency. The natural frequency is attained by dividing the resonance frequency by $\sqrt{1-D^2}$, where D is the measured damping ratio of the resonance peak.

Figure 4 (top) shows the unwrapped resonator structure. The split is modeled as a capacity and the coupling between transmission line and resonator structure is modeled as a current source. At first, a hypothetical case where the split capacity is $C = 0$ is considered. Here, the boundary condition for the current distribution of the standing wave on the resonator is $I = 0$ at the end of the open sides of the line (position of the split). Therefore, the half-wave length of the resonance frequency equals the circumference of the resonator, i.e., $\lambda_{\mathrm{res}1}/2 = 180\,\mathrm{mm}$, and thus the resonance wavelength is $\lambda_{\mathrm{res}1} = 360\,\mathrm{mm}$.

However, when adding a split capacity $C > 0$ to the open end of the line, the capacitor is charged with a charge Q and the current at the split becomes $|I| = |I_\mathrm{e}| > 0$, with $|I_\mathrm{e}| \sim Q$ or $|I_\mathrm{e}| \sim C$ respectively. As shown in Fig. 5, the capacity at the end of the line acts like an additional piece of line with a length of Δl, leading to an extension of the electrical length of the resonator (analogue to the electrical extension of dipole antennas through hat capacities). Therefore, the resonance wavelength increases ($\lambda_{\mathrm{res}2} = \lambda_{\mathrm{res}1} + 4\Delta l$) and the resonance frequency decreases to $f_{\mathrm{res}2} = v/\lambda_{\mathrm{res}2}$ respectively. Here v is the propagation velocity of the electromagnetic wave.

A quantitative description of the dependency between the extension of the electrical length Δl and the split capacity C can be found by calculating the input impedance of a transmission line of length l_0 terminated with the split capacity and equalizing this impedance with the input impedance of an open line (stub) of length $\lambda_{\mathrm{res}2}$.

According to transmission line theory, the input impedance of a transmission line with a length l_0 terminated with an impedance Z_2 at the resonance frequency $f_{\mathrm{res}2}$ is

$$Z_1 = Z_L \frac{Z_2 + jZ_L \tan\left(2\pi \frac{l_0}{\lambda_{\mathrm{res}2}}\right)}{Z_L + jZ_2 \tan\left(2\pi \frac{l_0}{\lambda_{\mathrm{res}2}}\right)}. \quad (1)$$

Here, Z_L is the wave impedance of the resonator structure and Z_2 is the impedance of the split capacity, i.e.,

$$Z_2 = \frac{1}{j2\pi f_{\mathrm{res}2} C}. \quad (2)$$

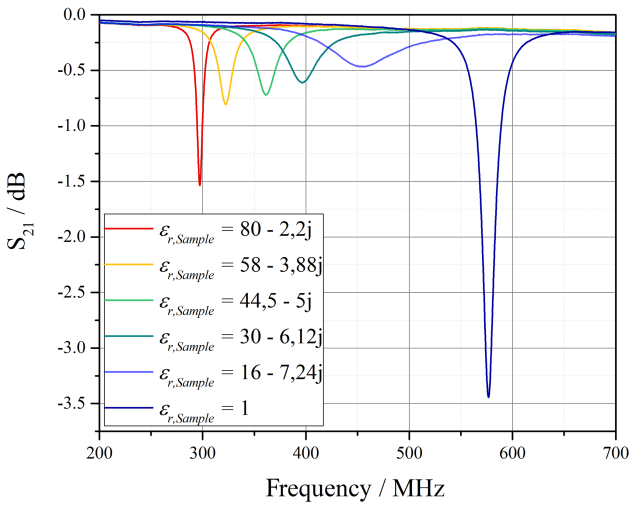

Figure 7. Transmission measurement for different mixtures of water and isopropanol in the sample container.

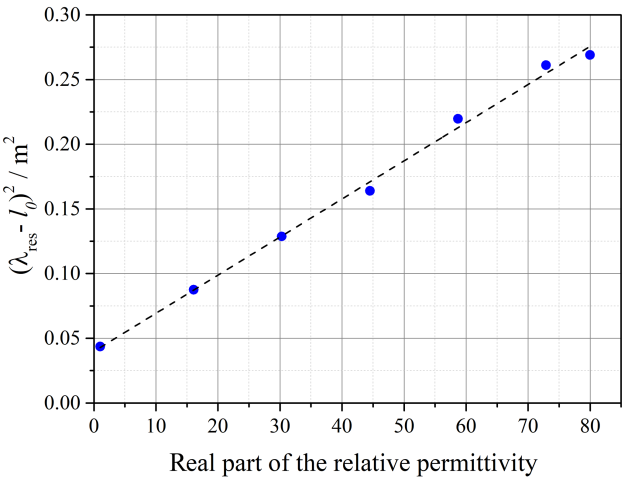

Figure 8. Validation of theory via measurements of water-isopropanol mixtures.

The electric potential in the center of the split is always $\varphi = 0\,\mathrm{V}$, because the open ends of the resonator are always on opposite potential. Therefore, for modulating the split as an equivalent circuit, the cross section depicted in Fig. 6 shows a transmission line connected to ground via three parallel capacities: the sample-dependent capacity C_{sample} and two parasitic capacities above and below the sample capacity $C_{\mathrm{air}} + C_{\mathrm{substrate}} = C_{\mathrm{p}}$.

Then, the split capacity C can be written as

$$C = C_{\mathrm{sample}} + C_{\mathrm{p}} = C_{\mathrm{sample},\ \varepsilon_{\mathrm{r}}=1} \cdot \varepsilon'_{\mathrm{r,\ sample}} + C_{\mathrm{p}}. \tag{3}$$

Here, $C_{\mathrm{sample},\varepsilon_r=1}$ is the sample capacity for an air-filled split. Combining Eqs. (1), (2) and (3), equalizing the result to the impedance of an open transmission line with length $l_1 = \lambda_{\mathrm{res2}}/4$ (resonance case: $Z_{\mathrm{res}} = 0$) and using a Taylor approximation yields the desired dependency between the resonance wavelength λ_{res2} and the relative sample permittivity ε_{r}':[1]

$$\lambda_{\mathrm{res2}} = 2l_0 + \sqrt{4l_0^2 + 16l_0 v Z_L (C_{\mathrm{p}} + C_{\mathrm{sample},\ \varepsilon_{\mathrm{r}}=1} \cdot \varepsilon'_{\mathrm{r,\ sample}})}. \tag{4}$$

Here v is the propagation velocity, which only depends on the speed of light c_0 and the effective permittivity $\varepsilon_{\mathrm{eff}}$, which in this term is a superposition of the relative substrate permittivity ($\varepsilon_{\mathrm{r,FR4}} = 4.1$) and the relative permittivity of air ($\varepsilon_{\mathrm{r\ ,Air}} = 1$):

$$v = \frac{c_0}{\sqrt{\varepsilon_{\mathrm{eff}}}}. \tag{5}$$

[1] Detailed calculation including single steps can be found in the Supplement.

Note that when $C = 0$, Eq. (4) becomes

$$\frac{\lambda_{\mathrm{res2}}}{4} = \frac{\lambda_{\mathrm{res1}}}{4} = l_0. \tag{6}$$

This result supports the theory, because, as was already shown in Fig. 4, for this hypothetical case, the half-wave length of the resonance frequency must be equal to the circumference of the resonator.

To further test Eq. (4) for plausibility, mixtures of isopropanol ($\varepsilon'_{\mathrm{r,i}} = 9$) with an increasing content of deionized water ($\varepsilon'_{\mathrm{r,w}} = 80$) are filled in the sample container, leading to a sample with increasing relative permittivity. The relative permittivity dependent on the mixture ratio can be found using Akerlof (1932), Sihvola (2000) and Lou et al. (1997).

It can be seen in Fig. 7 that increasing the real part of the relative permittivity of the sample $\varepsilon_{\mathrm{r,\ sample}}$ leads to an increase in resonance wavelength λ_{res2}, as predicted by Eq. (4), and thus to a shift in resonance frequency towards lower frequencies. Observing the peak width dependent on the imaginary part of the relative permittivity reveals that an increase in dielectric losses or conductivity leads to peak-broadening, i.e., lowering of the quality factor or increase in damping of the resonator.

With the data from Fig. 7, Eq. (4) is verified and the unknown capacities C_{p} and $C_{\mathrm{sample},\varepsilon_r=1}$ are determined. Therefore, the function is fitted to the measured data. As a linear fit delivers better results as a fit to a square root, Eq. (4) is squared to

$$(\lambda_{\mathrm{res2}} - 2l_0)^2 = 4l_0^2 + 16l_0 v Z_L C_{\mathrm{p}} + 16l_0 v Z_L C_{\mathrm{sample},\varepsilon_{\mathrm{r}}=1} \cdot \varepsilon'_{\mathrm{r,\ sample}}. \tag{7}$$

Figure 8 shows the left part of Eq. (7), i.e., $(\lambda_{\mathrm{res2}}–2l_0)^2$, dependent on the real part of the relative permittivity of the

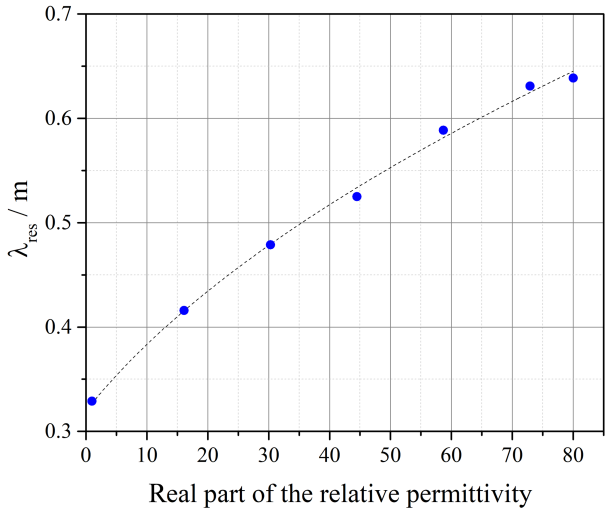

Figure 9. Dependency between the resonance wavelength and the real part of the relative permittivity.

sample $\varepsilon'_{\mathrm{r,\,sample}}$. The length l_0 is the half circumference of the used resonator structure (here, $l_0 = 90\,\mathrm{mm}$). To eliminate the influence of damping on the resonance frequency, the resonance wavelength is calculated to $\lambda_{\mathrm{res2}} = \frac{c_0}{f_0\sqrt{\varepsilon_{\mathrm{eff}}}}$ with $f_{\mathrm{res}} = f_0\sqrt{1-D^2}$.

A linear correlation with a Pearson's coefficient of $R = 0.999$ for the dependency between $(\lambda_{\mathrm{res2}}–2l_0)^2$ and the real part of the relative sample permittivity can be derived, confirming the theoretical considerations. Determination of C_{p} and $C_{\mathrm{sample},\varepsilon_r=1}$ is achieved via equating coefficients with the linear fit to

$$C_{\mathrm{p}} = \frac{a - 4l_0^2}{16 l_0 v Z_L} = 2.792\ \mathrm{pF}\ \text{ and}$$
$$C_{\mathrm{sample},\varepsilon_{\mathrm{r}}=1} = \frac{b}{16 l_0 v Z_L} = 0.213\ \mathrm{pF}. \qquad (8)$$

Therefore, all variables included in Eq. (4) are determined and calculating the resonance frequency for a given sample permittivity is possible. Concluding, Fig. 9 shows the dependency between the resonance wavelength and the real part of the relative permittivity.

These results enable a target-oriented optimization process. From Eq. (4) it can be seen that the sensitivity depends on the split capacity, the wave impedance, the circumference of the resonator structure and the propagation velocity. In the next section, a systematic study of these parameters is performed to increase the sensitivity of the setup.

4 Setup optimization

The propagation velocity only depends on the speed of light c_0 and the effective permittivity $\varepsilon_{\mathrm{eff}}$. To increase the sensitivity, v would have to be increased, which is only possible by decreasing the effective permittivity and thus decreasing the relative permittivity of the substrate. As $\varepsilon_{\mathrm{r,FR4}}$ has already a low value, the propagation velocity is not a parameter with broad potential for optimization. On the other hand, increasing the split capacity is more effective which is presented in the following section.

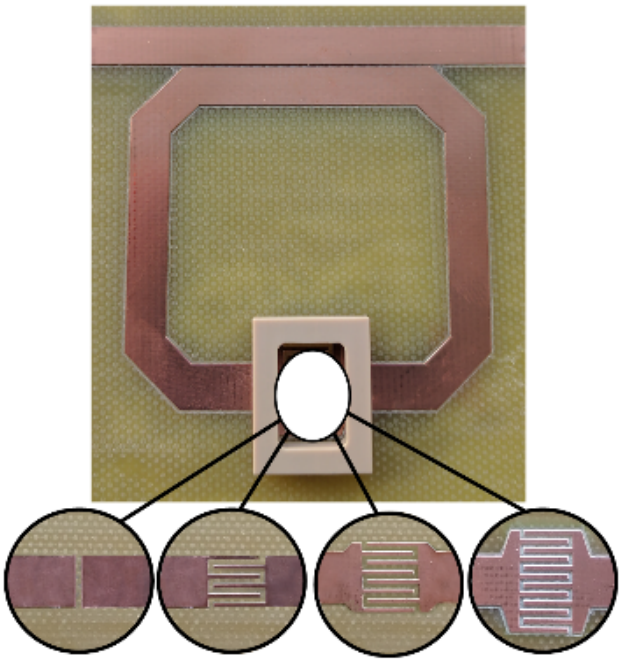

Figure 10. Split-ring resonator with different split capacities.

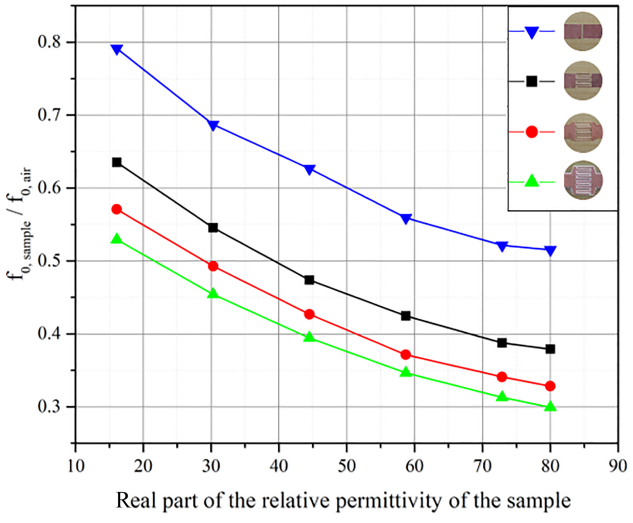

Figure 11. Measuring an increasing sample permittivity with different split capacities.

Figure 10 shows the split-ring resonator with different split capacities. To increase C, interdigital structures are used, instead of a single split. The number of interdigital fingers is gradually increased from three per side to six per side. The

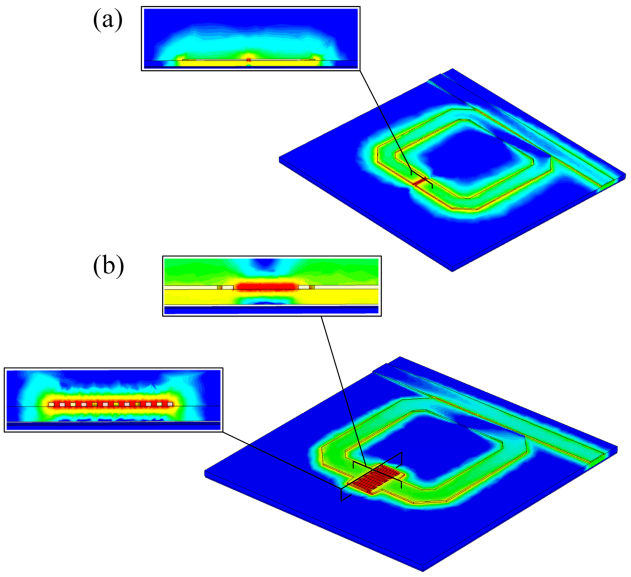

Figure 12. Electrical field in the cross section of the split capacity for a simple split **(a)** and interdigital structure **(b)**.

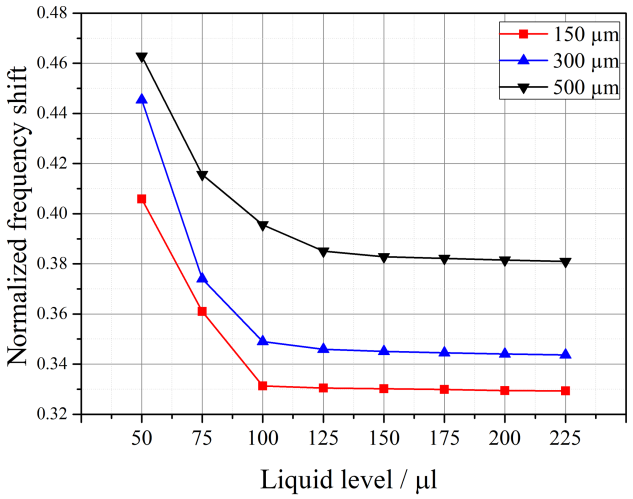

Figure 13. Decreasing penetration depth via decreasing the space between the fingers of an interdigital structure.

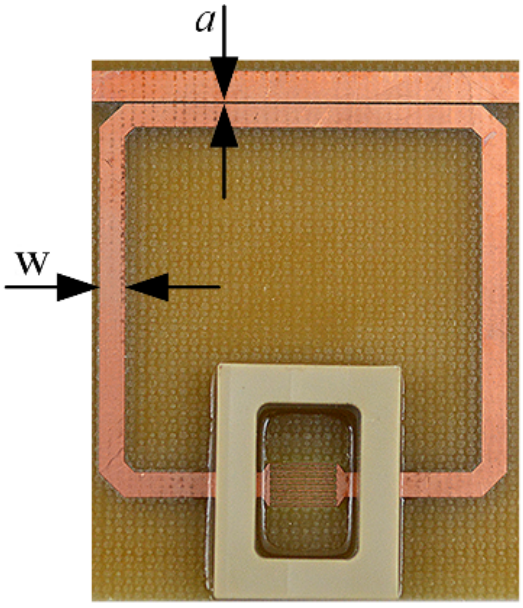

Figure 14. Split-ring resonator on a 1.4 mm thick FR4 substrate with six-finger interdigital capacity.

fingers have a length[2] of $l = 5$ mm, a width of $w_f = 500$ µm and the space between the fingers of $s = 500$ µm.

To investigate the effect on the sensitivity, again mixtures of isopropanol and deionized water are measured. The results are shown in Fig. 11. Here, the resonance frequencies are normalized to the resonance frequency of the unloaded resonator.

Increasing the split capacity leads to a significantly increased sensitivity. When using a simple split, the relative frequency shift from the unloaded resonator ($\varepsilon_{r,\,sample} = 1$) to the resonator loaded with deionized water ($\varepsilon_{r,\,sample} = 80$) is 50 %, while the relative frequency shift increases to 70 % when using an interdigital structure with six fingers.

Another advantage of interdigital structures for the realization of a biosensor becomes apparent by looking at the electrical field in the capacity, depicted in Fig. 12. When using a simple split, the penetration depth of the electrical field is relatively high. Therefore, the environment (e.g., permittivity of the sample) has a high influence on the measurement. However, the purpose of a biosensor is to detect binding reactions on the surface of the split capacity and therefore a low penetration depth is preferable to increase the influence of the binding reaction and decrease the influence of the environment on the measuring result. Therefore, the six-finger interdigital structure is superior to the simple split, as the field concentrates around the fingers, see Fig. 12b.

To further decrease the penetration depth and simultaneously increase the capacity, the space between the fingers of the six-finger structure is gradually decreased from $s = 500$ µm to $s = 150$ µm in the final optimization step. Smaller spaces s between the fingers could not be investigated due to technical limitations in the manufacturing process.

To visualize the effect on the penetration depth, the fluid level in the sample container is gradually increased and the resonance frequency is observed. Due to its low surface tension, this experiment is carried out with dimethyl sulfoxide (DMSO) with a relative permittivity of $\varepsilon_{r,sample} = 46.7$. However, note that for low fluid levels (volumes of 50 and 75 µL) a complete and even wetting of the split capacity cannot be

[2] Increasing the length of the fingers has a similar effect to increasing the number of fingers. A figure comparing results for $l = 5$ mm and $l = 3.5$ mm can be found in the Supplement.

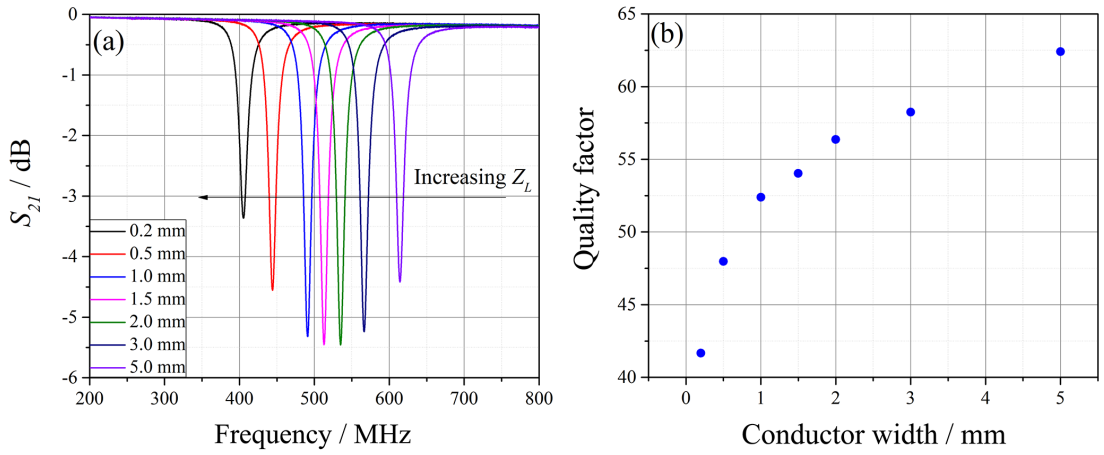

Figure 15. Measurement results for unloaded resonators with different wave impedances of the resonator structure: **(a)** transmission measurement; **(b)** quality factor.

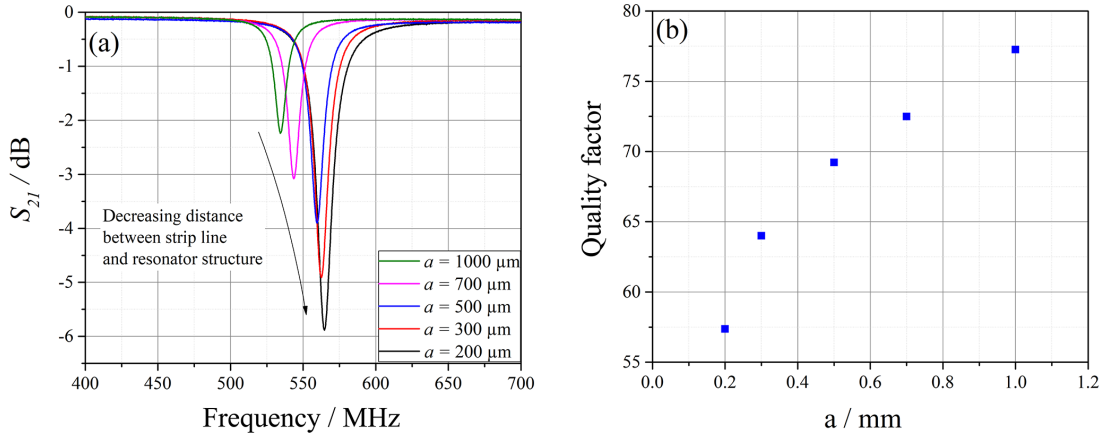

Figure 16. Increasing coupling by decreasing distance between strip line and resonator structure: **(a)** transmission measurement; **(b)** quality factor.

guaranteed, as the volume of the sample container is significantly larger than that of the fluid, resulting in higher measurement uncertainty at those measurement points.

The results in Fig. 13 show that decreasing the space between the fingers leads to an increased split capacity and thus to an increased sensitivity, as there is a higher shift in resonance frequency towards smaller s. Furthermore, the penetration depth decreases: while there is still a small frequency shift observable for the resonator with $s = 500\,\mu\text{m}$, when increasing the fluid level from 200 to 250 µL, the signal already saturates at a fluid level of 100 µL for the resonator with $s = 150\,\mu\text{m}$.

In the first experiments, we found that using a 3 mm thick FR4 substrate relates to significant fabrication tolerances. Therefore, we chose to carry out all following experiments with split-ring resonators on 1.5 mm thick FR4 substrates. The corresponding split-ring resonator is shown in Fig. 14.

The wave impedance is in inverse proportion to the conductor width of the resonator structure ($Z_L \sim 1/w$). Figure 15 depicts the S_{21} dependent on the frequency for resonators with decreasing w and therefore increasing Z_L of the square resonator structure. The width of the transmission line is kept constant at 2.4 mm (50 Ω on 1.5 mm FR4 substrate) for all measurements. As predicted by Eq. (4), an increasing Z_L leads to a decreasing resonance frequency. However, a $w < 1.5$ mm leads deterioration of the coupling between transmission line and resonator structure; i.e., the minimum S_{21} becomes smaller. Additionally, the quality factor decreases with increasing Z_L. Therefore, the optimum width of the resonator structure is found at $w \approx 2.0$ mm as the quality factor is not significantly reduced, combined with maximum coupling.

One option to increase coupling between strip line and resonator structure is to decrease their distance a (see Fig. 14). The distance a is gradually decreased from $a = 1000\,\mu\text{m}$ to

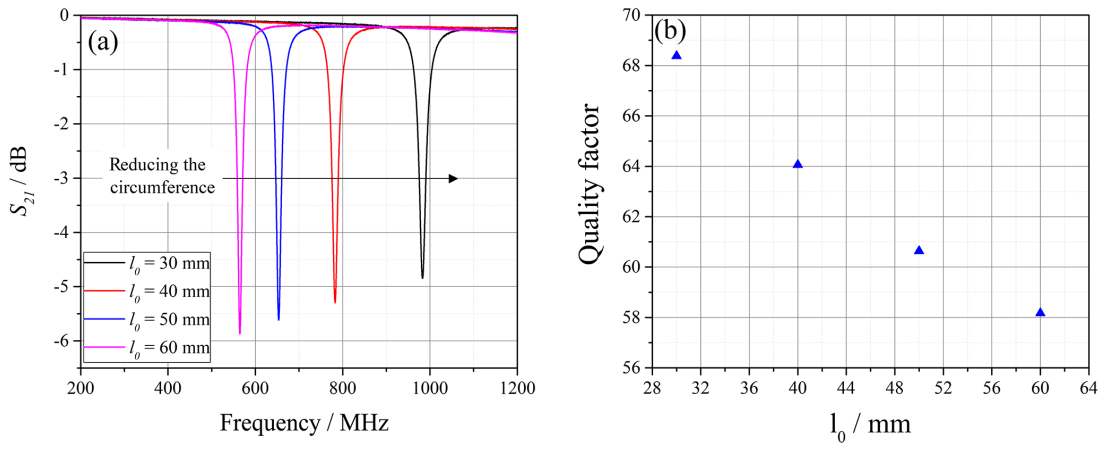

Figure 17. Influence of the circumference of the resonator structure on the resonance frequency: **(a)** transmission measurement; **(b)** quality factor.

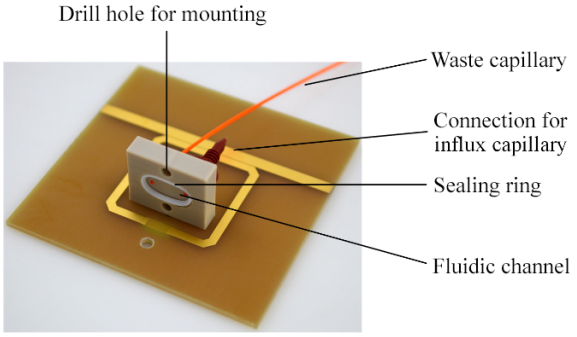

Figure 18. Final layout of the split-ring resonator.

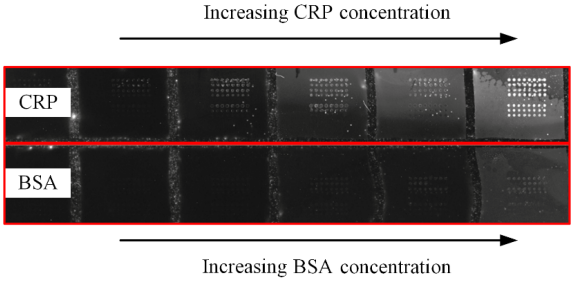

Figure 19. Optical detection of CRP bound to aptamers.

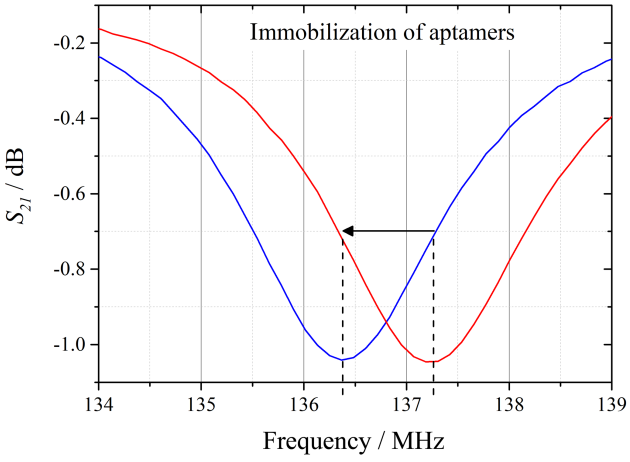

Figure 20. S_{21} with deionized water as sample before and after immobilization of aptamers.

$a = 200\,\mu m$. Smaller distances could not be investigated due to technical limitations in the manufacturing process.

Figure 16 shows the measured transmission of resonators with different a. Decreasing the distance leads to better coupling but decreases the quality factor of the resonance peak. However, directly contacting transmission line and resonator structure (data not shown) leads to even higher coupling but also to massive peak deformation.

Finally, the circumference ($2\,l_0$) of the resonator structure influences the sensitivity according to Eq. (4). Furthermore, it is possible to adjust the resonance frequency, as shown in Fig. 17. A length of $l_0 = 30\,mm$ leads to a resonance frequency of almost 1 GHz, while doubling l_0 reduces it to 570 MHz. Higher quality factors are found at higher resonance frequencies.

The final layout of the split-ring resonator, based on the presented investigations, is depicted in Fig. 18. The resonator is equipped with a fluidic channel to enable automated measurements with a syringe pump. The distance between strip line and resonator structure is $a = 100\,\mu m$ and the circumference is $2\,l_0 = 100\,mm$. Furthermore, the conducting areas, especially the split capacity, are chemically coated with gold to enable an immobilization of aptamers to perform a preliminary investigation of the split-ring resonator as a biosensor, which is described in the following section.

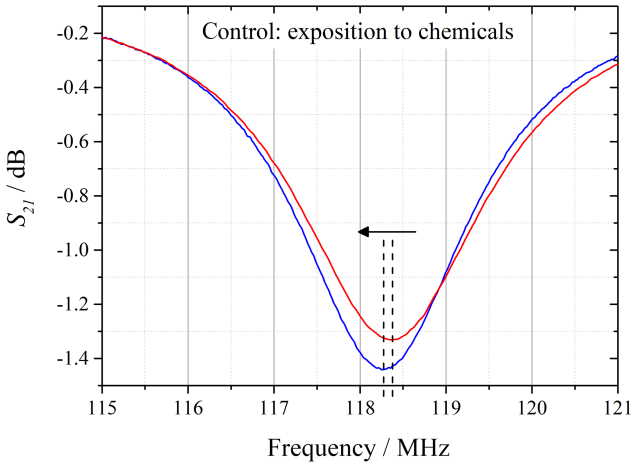

Figure 21. S_{21} of control resonator with deionized water as sample before and after exposure to immobilization chemicals.

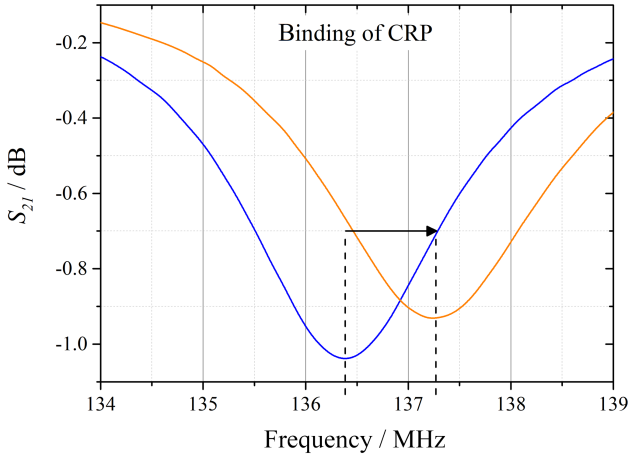

Figure 22. S_{21} with deionized water as sample before and after binding of CRP.

5 Initial results: aptamer-based detection of C-reactive protein (CRP) with a split-ring resonator

In this section, the split capacity is functionalized with aptamers. Aptamers can be considered as artificial alternatives to antibodies, produced via chemical synthesis (Toh et al., 2015). Their in vitro selection process enables the generation of different aptamers selectively binding a huge variety of different target molecules, even toxic or low immunogenic ones (Mairal et al., 2008). As a first model system, CRP purified from human plasma (Bio-Rad, Puchheim, Germany) and corresponding aptamers (sequences derived from Chao-June Huang et al., 2010, and synthesized by BioSpring, Frankfurt, Germany) are purchased from OTC Biotech, San Antonio, USA. In a first step, the aptamers' ability to selectively bind CRP is tested. Therefore, 5′ amino-modified

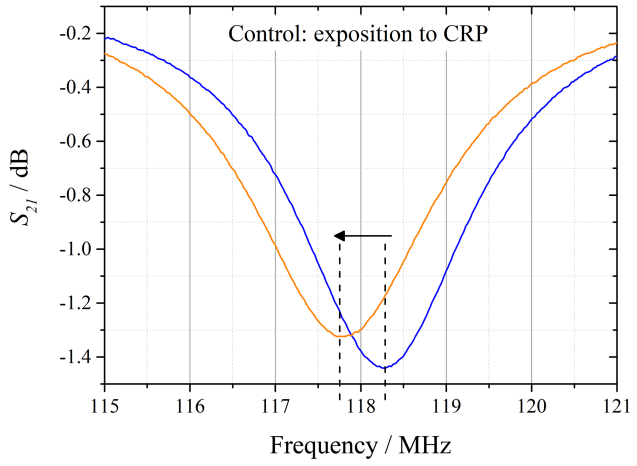

Figure 23. S_{21} with deionized water as sample before and after exposition to CRP.

aptamers are spotted on a 3-D aldehyde-modified microarray slide (PolyAn, Berlin, Germany), similar to the procedure described in Heilkenbrinker et al. (2015), and subsequently exposed to solutions with different concentrations of fluorescence-labeled CRP to perform quantitative measurements.

Furthermore, the aptamers are exposed to solutions with different concentrations of fluorescence-labeled bovine serum albumin (BSA) to test the selectivity of the aptamers.

The results in Fig. 19 show that the fluorescence of the small spots where aptamers are immobilized increases when exposed to an increasing concentration of fluorescence-labeled CRP. Therefore, it can be concluded that quantitative measurements of CRP are possible with these aptamers. The test series with fluorescence-labeled BSA shows virtually no response, which leads to the conclusion that the aptamer selectively binds CRP.

Similar to the immobilization procedure described in Loo et al. (2014), aptamers are immobilized on the split capacity of a split-ring resonator. In parallel, a control resonator is exposed to all chemicals necessary for the immobilization process without finally immobilizing aptamers. In this way it is excluded that the sensor response arises from parasitic effects, e.g., an alteration of the capacity, due to reactions with those chemicals. Furthermore, all measurements are carried out with deionized water in the sample container after performing several washing steps. Thus, the influence of the permittivity of the solutions containing aptamers and CRP respectively is eliminated and it is assured that solely binding reactions on the surface of the split capacity are causing a measuring signal.

Figure 20 shows that the immobilization of aptamers leads to a lower resonance frequency. This can be explained by a good polarizability of the aptamers due to their exposed negative charges. The control resonator shows virtually no

response after being exposed to the chemicals used for the immobilization process (see Fig. 21).

Subsequently, both split-ring resonators are exposed to a 1 µM CRP-containing solution. The resonator with immobilized aptamers shows a shift in resonance frequency back towards higher frequencies (Fig. 22). A sound explanation is that the formerly exposed charges of the aptamers are enclosed and neutralized in the aptamer–CRP binding complex and therefore the polarizability is significantly decreased. Another factor for a decreased polarizability can be the higher mass of the aptamer–CRP binding complex compared to the unbound aptamer.

The control sensor shows an inverse behavior, see Fig. 23: the resonance frequency increases after exposure to CRP. This can be caused by adsorption of CRP on the gold surface, leading to an increase in split capacity.

However, the presented results show that aptamer-functionalized split-ring resonators can be used as biosensors, as the small changes in split capacity due to binding reactions on the gold surface can be detected via the highly sensitive detection of shifts in resonance frequency.

6 Conclusions

In this work, we presented a systematic investigation of a split-ring resonator for application as a biosensor. The parameters responsible for the sensitivity of the setup were determined based on a new approach to determine the resonance frequency dependent on the relative permittivity of the sample using transmission line theory. Based on these parameters, the resonator structure was optimized and all optimizations where verified by measurements. Subsequently, a split-ring resonator was functionalized with aptamers and a selective detection of CRP could be shown. In future work, the immobilization process will be improved to gain higher sensor responses and more efficient blocking of the gold surface. Furthermore, the optimal resonance frequency for CRP detection needs to be determined. Finally, quantitative measurements will be performed.

Data availability. All relevant data are contained in the paper and the Supplement.

The Supplement related to this article is available online at https://doi.org/10.5194/jsss-7-101-2018-supplement.

Competing interests. The authors declare that they have no conflict of interest.

Special issue statement. This article is part of the special issue "Sensor/IRS2 2017". It is a result of the AMA Conferences, Nuremberg, Germany, 30 May–1 June 2017.

Edited by: Robert Kirchner
Reviewed by: two anonymous referees

References

Akerlof, G.: Dielectric constants of some organic solvent-water mixtures at various temperatures, J. Am. Chem. Soc., 54, 4125–4139, https://doi.org/10.1021/ja01350a001, 1932.

Albishi, A. and Ramahi, O. M.: Detection of surface and subsurface cracks in metallic and non-metallic materials using a complementary split-ring resonator, Sensors (Basel, Switzerland), 14, 19354–19370, https://doi.org/10.3390/s141019354, 2014.

Ebrahimi, A., Withayachumnankul, W., Al-Sarawi, S., and Abbott, D.: High-Sensitivity Metamaterial-Inspired Sensor for Microfluidic Dielectric Characterization, IEEE Sensors J., 14, 1345–1351, https://doi.org/10.1109/JSEN.2013.2295312, 2014.

Heilkenbrinker, A., Reinemann, C., Stoltenburg, R., Walter, J.-G., Jochums, A., Stahl, F., Zimmermann, S., Strehlitz, B., and Scheper, T.: Identification of the target binding site of ethanolamine-binding aptamers and its exploitation for ethanolamine detection, Anal. Chem., 87, 677–685, https://doi.org/10.1021/ac5034819, 2015.

Huang, Y. and Boyle, K.: Antennas, From theory to practice, Chichester, Wiley, 2008.

Huang, C.-J., Lin, H.-I., Shiesh, S.-C., and Lee, G.-B.: Integrated microfluidic system for rapid screening of CRP aptamers utilizing systematic evolution of ligands by exponential enrichment (SELEX), Biosensors and Bioelectronics, 25, 1761–1766, https://doi.org/10.1016/j.bios.2009.12.029, 2010.

Jaruwongrungsee, K., Waiwijit, U., Withayachumnankul, W., Maturos, T., Phokaratkul, D., Tuantranont, A., Wlodarski, W., Martucci, A., and Wisitsoraat, A.: Microfluidic-based Split-Ring-Resonator Sensor for Real-time and Label-free Biosensing, Proc. Eng., 120, 163–166, https://doi.org/10.1016/j.proeng.2015.08.595, 2015.

Lee, H.-J. and Yook, J.-G.: Biosensing using split-ring resonators at microwave regime, Appl. Phys. Lett., 92, 254103, https://doi.org/10.1063/1.2946656, 2008.

Lee, H.-J., Lee, H.-S., Yoo, K.-H., and Yook, J.-G.: DNA sensing using split-ring resonator alone at microwave regime, J. Appl. Phys. 108, 014908, https://doi.org/10.1063/1.3459877, 2010.

Lee, H.-J., Lee, J.-H., Moon, H.-S., Jang, I.-S., Choi, J.-S., Yook, J.-G., and Jung, H.-I.: A planar split-ring resonator-based microwave biosensor for label-free detection of biomolecules, Sensor. Actuator. B, 169, 26–31, https://doi.org/10.1016/j.snb.2012.01.044, 2012.

Loo, F.-C., Ng, S.-P., Wu, C.-M. L., and Kong, S. K.: An aptasensor using DNA aptamer and white light common-path SPR spectral interferometry to detect cytochrome-c for anticancer drug screening, Sensor. Actuator. B, 198, 416–423, https://doi.org/10.1016/j.snb.2014.03.077, 2014.

Lou, J., Hatton, T. A., and Laibinis, P. E.: Effective Dielectric Properties of Solvent Mixtures at Microwave Frequencies, J. Phys. Chem. A, 101, 5262–5268, https://doi.org/10.1021/jp970731u, 1997.

Mairal, T., Ozalp, V. C., Lozano Sánchez, P., Mir, M., Katakis, I., and O'Sullivan, C. K.: Aptamers. Molecular tools for analytical applications, Anal. Bioanal. Chem., 390, 989–1007, https://doi.org/10.1007/s00216-007-1346-4, 2008.

Naqui, J., Durán-Sindreu, M., and Martín, F.: Novel sensors based on the symmetry properties of split ring resonators (SRRs), Sensors (Basel, Switzerland), 11, 7545–7553, https://doi.org/10.3390/s110807545, 2011.

Puentes, M., Weiss, C., Schussler, M., and Jakoby, R.: Sensor array based on split ring resonators for analysis of organic tissues, edited by: IEEE Staff, 2011 IEEE/MTT-S International Microwave Symposium, 2011 IEEE/MTT-S International Microwave Symposium – MTT 2011, Baltimore, MD, USA, 5/6/2011–10/6/2011, IEEE Staff, IEEE, 1–4, 2011.

Reinecke, T., Ahrens, S., and Zimmermann, S.: Biosensorplattform auf Basis von Split-Ring Resonatoren, edited by: Zimmermann, S., 30, Messtechnisches Symposium, Berlin: De Gruyter, De Gruyter Oldenbourg, 2016.

Reinecke, T., Kobelt, T., Ahrens, A., Zimmermann, S., Scheper, T., and Walter, J.-G. (Eds.): A3.4 – Biosensor based on a split-ring resonator, AMA Service GmbH, Von-Münchhausen-Str. 49, 31515 Wunstorf, Germany, 6 pp., AMA Association for Sensors and Measurement, Sophie-Charlotten-Str. 15, 9 Berlin, Germany, 2017.

Rudge, A. W., Milne, K., Olver, A. D., and Knight, P. (Eds.): The Handbook of Antenna Design, London, Peregrinus (IEE electromagnetic waves series, 16), 1983.

Schueler, M., Mandel, C., Puentes, M., and Jakoby, R.: Metamaterial Inspired Microwave Sensors, IEEE Microwave, 13, 57–68, https://doi.org/10.1109/MMM.2011.2181448, 2012.

Sihvola, A.: Mixing Rules with Complex Dielectric Coefficients, Subsurf. Sens. Technol. Appl., 1, 393–415, https://doi.org/10.1023/A:1026511515005, 2000.

Smith, D. R., Padilla W. J., Vier, D. C., Nemat-Nasser, C., and Schultz, S.: Composite medium with simultaneously negative permeability and permittivity, Phys. Rev. Lett., 84, 4184–4187, https://doi.org/10.1103/PhysRevLett.84.4184, 2000.

Toh, S. Y., Citartan, M., Gopinath, S. C. B., and Tang, T.-H.: Aptamers as a replacement for antibodies in enzyme-linked immunosorbent assay, Biosens. Bioelectron., 64, 392–403, https://doi.org/10.1016/j.bios.2014.09.026, 2015.